The interconnection between independent reactive control policies drives the stringency of local containment

Adriana Reyna-Lara [a,b,1], David Soriano-Paños [b,c,1], Alex Arenas [d], Jesús Gómez-Gardeñes [a,b,e,*]

[a] Department of Condensed Matter Physics, University of Zaragoza, E-50009 Zaragoza, Spain
[b] GOTHAM Lab–Institute for Biocomputation and Physics of Complex Systems (BIFI), University of Zaragoza, E-50018 Zaragoza, Spain
[c] Instituto Gulbenkian de Ciência, 2780-156 Oeiras, Portugal
[d] Departament d'Enginyeria Informàtica i Matemàtiques, Universitat Rovira i Virgili, 43007 Tarragona, Spain
[e] Center for Computational Social Science (CCSS), Kobe University, 657-8501 Kobe, Japan

ARTICLE INFO

ABSTRACT

The lack of medical treatments and vaccines upon the arrival of the SARS-CoV-2 virus has made non-pharmaceutical interventions the best allies in safeguarding human lives in the face of the COVID-19 pandemic. Here we propose a self-organized epidemic model with multi-scale control policies that are relaxed or strengthened depending on the extent of the epidemic outbreak. We show that optimizing the balance between the effects of epidemic control and the associated socio-economic cost is strongly linked to the stringency of control measures. We also show that non-pharmaceutical interventions acting at different spatial scales, from creating social bubbles at the household level to constraining mobility between different cities, are strongly interrelated. We find that policy functionality changes for better or worse depending on network connectivity, meaning that some populations may allow for less restrictive measures than others if both have the same resources to respond to the evolving epidemic.

1. Introduction

Upon the arrival of any contagious disease, when nothing is known about the epidemiological features of the new transmissible pathogen or no drugs or vaccines are available, the authorities must resort to non-pharmaceutical interventions (NPIs) to keep the epidemic outbreak under control. Such a scenario has been reflected by the irruption of the COVID-19 pandemic where NPIs have been fundamental to shape the transmission dynamics of the SARS-CoV-2 virus worldwide, helping to reduce its already elevated impact on the population [1]. Nonetheless, the specific intervention was chosen to cope with the pandemic and the degree of accomplishment of the different measures notoriously varied from one country to another, depending on different social, economic, political or geographic features [2,3]. While some countries located in South-East Asia or Oceania were capable of maintaining low levels of community transmission via the timely combination of strict border closure policies, robust contact tracing systems and punctual local lockdowns to eradicate localized outbreaks, most of the countries worldwide reacted with population-wide lockdowns as an urgent solution to the exponentially growing number of local contagions [4].

However, widespread lockdowns to contain the COVID-19 pandemic have disrupted the world economy [5]. School and business closures, restrictions on international travel, and trade have led to massive job losses and the worst GDP contraction in decades in most of these countries [6–8]. Even though vaccines have given some relief to both health and economic systems relaxing restrictions in some countries, the unequal distribution and adoption of vaccines worldwide [9,10], along with their reduced efficiency to the new variants of the virus [11,12], prevent countries from completely abandoning NPIs as efficient tools against the ongoing pandemic. Moreover, fearing the extending human toll with renewed waves caused by new variants of the virus, policymakers have drawn on lockdowns, stay-at-home and self-quarantine programs over and over again [13]. The multi-layered crisis that primarily encompasses the health and economic systems requires joint effective policies to prevent worse outcomes. An optimal policy response has to face the challenge of reducing the daily incidence of the disease allowing health care systems to cope while reshaping their economies by adjusting the mobility restrictions.

Several models have addressed targeted lockdowns to optimize the economic losses and the epidemic control [14–16]. Others have attempted to promote sustainable policies alternating [17] or intermittently implementing [18] control measures that allow the economic

---

* Corresponding author at: Center for Computational Social Science (CCSS), Kobe University, 657-8501 Kobe, Japan.
E-mail address: gardenes@unizar.es (J. Gómez-Gardeñes).
[1] These two authors have contributed equally to this work.

system to cope while giving relief to the health systems. The different policy scenarios were simulated to analyze both health and economic effects [19]. However, these models do not account for the importation of new cases from other places that may spark a new outbreak or epidemic wave, most of them do not include human mobility, and the important effect of social reactions to the policies implemented [20–22].

Here, we propose a new theoretical framework to explore the interplay between the spread of infectious diseases and closure interventions promoted to keep the outbreaks under control and their economic consequences. The main novelty of this formalism is that the latter interventions are strongly coupled with the dynamical state of the system, being their implementation and strength adapted to the evolution of an epidemic outbreak. We perform a multiscale approach by acting on the processes driving the spread of the disease across different spatial scales, ranging from the spatial diffusion of cases due to commuting mobility between municipalities to the local transmission events fostering the community transmission of the pathogen. Our results highlight that these different spatial scales are not independent one from another, stressing the need to use systemic approaches to achieve an optimal trade-off between the strength of the control policies, their benefits for the health system and their associated socioeconomic cost.

2. The model

Metapopulations constitute a natural avenue to simultaneously capture the community transmission of the virus, as the internal dynamics of each patch, and its spatial diffusion as a result of the mixing events of the individuals from different subpopulations. Here we consider an extension of the Movement-Interaction-Return (MIR) model [23] to accommodate household interactions [24] and complex compartmental dynamics [25]. As such, the MIR model comprises three stages: the first (M) is associated with mobility flows whereas the last two (I and R) are associated with possible contagions either at the destination (I) or at the household (R).

To implement contagion processes occurring at stages I and R we make use of a tailored model for the spread of SARS-CoV-2. This model contains the following compartments: Susceptible (S), Exposed (E), Presymptomatic infectious (P), Asymptomatic infectious (A), symptomatic Infectious (I), Detected (D), and Recovered (R). The transition probabilities between each of the former compartments are represented Fig. 1.A and explained in detail below. In its turn stage M of the MIR model assumes that the whole population of N individuals is divided into N_P subpopulations, each one associated with a specific geographic location (patch) i and of size n_i ($N = \sum_{j=1}^{N_P}$). The population n_i of each patch i corresponds to the number of residents asscoiated with the corresponding geographic area as dictated by census information. To capture the daily mobility patterns of the population, we assume that the population moves according to the Origin-Destination (OD) matrix $bf\mathbf{R}$, whose elements R_{ij} reflects the probability that a resident in patch i moves from patch i to patch j as shown in Fig. 1.B.

Finally, the main novelty of the model resides in the autonomous control policies which are either strengthened or relaxed as a function of the dynamical advance of the outbreak. In particular, at each patch i, we define a parameter $p_i(t)$ that determines the share of the population working actively and carrying out their usual social life. As shown in Fig. 1.C this parameter depends on the fraction of detected residents, hereinafter denoted by $\rho_i^D(t)$. When this fraction is below a certain tolerance threshold, ε, a patch follows a normal socioeconomic activity level ($p_i=1$). However, when $\rho_i^D(t) > \varepsilon$ different interventions are activated to reach the desirable control of the disease, being the extent of the contention measures captured by the value of $p_i<1$. Mimicking different real policies implemented during the course of COVID-19 pandemic, we consider the following interventions affecting different resolution levels:

1. At the metapopulation level, usual mobility patterns, encoded in matrix $\mathbf{R}$, are altered to minimize the interactions with the population from those areas with a high incidence numbers ($\rho_j^D > \varepsilon$). This way the probability that a patch j with high incidence at time t (and hence low $p_j(t)$) receives commuters from patch i decreases as $p_j(t) R_{ij}$.

2. Apart from receiving fewer visitors, the economic activity of a patch j with a high incidence is modulated according to the extent of the disease in its population. This way, a fraction $p_j(t)$ of residents in patch j
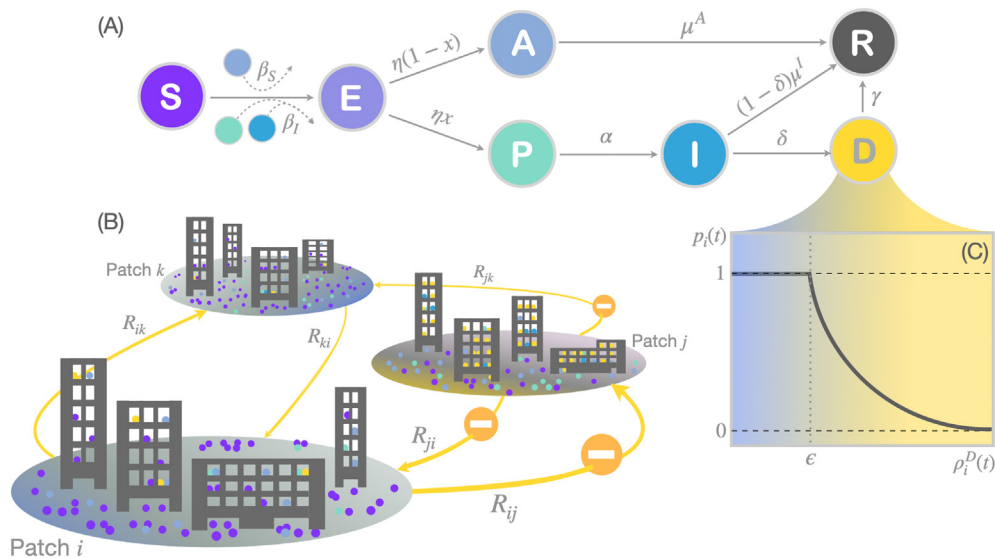

Fig. 1. Scheme of the multiscale reactive control model. A. The compartmental model comprises 7 compartments. Susceptible individuals (S) can be infected by infectious agents in asymptomatic (A), presymptomatic (P) and symptomatic (I) compartments. Once infected, agents pass to an exposed (E) compartment before passing to either asymptomatic (A) or symptomatic. In the latter case agents transit first a presymptomatic (P) stage before developing symptoms (I). A symptomatic agent can be detected (D) before being removed (R) or, otherwise, directly pass to R, which is the final compartment for those asymptomatic. B. In the metapopulation model individuals interact both inside and outside households. The activity outside households takes place in the residential patch or in a different one through the movement of individuals. Mobility flows between patches are ruled by matrix $\mathbf{R}$ whose elements R_{ij} account for the probability that a resident in patch i visits j. C. When the fraction of D in a patch i exceeds some threshold ε the activity level of the patch p_i decreases, affecting both the mobility and the social contacts of agents.

follows a normal socioeconomic activity while the remaining $(1-p_j(t))$ fraction are set to inactive and reduce their interactions to those taking place at the household level.

3. Finally, the reduction of the economic activity of the population has been usually accompanied by measures aimed at creating social bubbles preventing the transmission of the disease between members from different households. Note that this mechanism demands the creation of a new compartment CH to accommodate those susceptible individuals without infectious individuals in their social bubbles and, therefore, protected from the disease. Likewise, to model the efficiency of this mechanism, we introduce a new parameter, the social permeability ϕ, denoting the fraction of households whose members are not efficiently isolated [26], despite being inactive from the socioeconomic point of view.

In the following we describe the equations capturing the three mechanisms that interplay in the metapopulation model. Namely, the compartmental dynamics, the mobility of agents, and the reactive containment policies.

2.1. Coupling contagion and commuting dynamics

As shown in Fig. 1.A the compartmental model at work includes 7 epidemiological compartments in an attempt to capture those epidemiological states that are relevant for addressing SARS-CoV-2 transmission and the associated non-pharmaceutical interventions. The different transitions between these 7 compartments are as follows. First, susceptible (S) agents can be infected by contact with presymptomatic (P), asymptomatic (A) and infected (I) agents with probability β^c, $c \in \{\textbf{P}, \textbf{A}, \textbf{I}\}$. If infected, susceptible agents turn exposed (E), for an average period of η^{-1} days. It is then assumed that a fraction x of the population becomes symptomatic while the remaining fraction $(1-x)$ becomes asymptomatic (A). The former visit the presymptomatic but infectious stage for an average period of α^{-1} days before becoming symptomatic and infectious (I). Symptomatic and asymptomatic infectious individuals are assumed to overcome the disease with probabilities μ^I and μ^A respectively. In the case of symptomatic individuals, we assume that they can be detected (D) with probability δ and, once identified, detected individuals are perfectly isolated and assumed not to transmit the disease accordingly. Finally, to control the time one detected individual is identified as an active case, we assume that they pass to the R compartment with probability γ.

The interplay between contagion processes contained in the former epidemiological dynamics and human mobility is modeled with a Microscopic Markov Chain Approach [27]. To this aim, we assume that each time step corresponds to a day and each patch i is characterized by a set of variables $\rho_i^m(t)$ that govern the fraction of the residents in compartment m at time t. Following the premises of the compartmental dynamics and the recurrent nature of human mobility flows, these equations read:

$$\rho_i^S(t+1) = \left[\rho_i^S(t) + \rho_i^{CH}(t)\right]\left[p_i(t)(1-\Pi_i^{act}(t)) + (1-p_i(t))(1-sh_i)\left(1-\Pi_i^{in}(t)\right)\right], \tag{1}$$

$$\rho_i^{CH}(t+1) = \left[\rho_i^S(t) + \rho_i^{CH}(t)\right](1-p_i(t))sh_i, \tag{2}$$

$$\rho_i^E(t+1) = \left[\rho_i^S(t) + \rho_i^{CH}(t)\right]\left[p_i(t)\Pi_i^{act}(t) + (1-p_i(t))(1-sh_i)\Pi_i^{in}(t)\right] \\ + (1-\eta)\rho_i^E(t), \tag{3}$$

$$\rho_i^P(t+1) = (1-\alpha)\rho_i^P(t) + \eta x \rho_i^E(t), \tag{4}$$

$$\rho_i^A(t+1) = \left(1-\mu^A\right)\rho_i^A(t) + \eta(1-x)\rho_i^E(t), \tag{5}$$

$$\rho_i^I(t+1) = (1-\delta)(1-\mu^I)\rho_i^I(t) + \alpha\rho_i^P(t), \tag{6}$$

$$\rho_i^D(t+1) = (1-\gamma)\rho_i^D(t) + \delta\rho_i^I(t), \tag{7}$$

$$\rho_i^R(t+1) = \rho_i^R(t) + (1-\delta)\mu^I\rho_i^I(t) + \mu^A\rho_i^A(t) + \gamma\rho_i^D(t), \tag{8}$$

where sh_i represents the probability that a confined susceptible resident of patch i is isolated in a completely susceptible household. This happens when all the members of the household are not infectious and not mixed with the rest of households. Therefore

$$sh_i(t) = \left(1-\rho_i^E(t)-\rho_i^P(t)-\rho_i^A(t)-\rho_i^I(t)\right)^{\sigma_i-1}(1-\phi), \tag{9}$$

where σ_i is the average size for the households located inside the population i.

The former set of equations contains the terms Π_i^{act} and Π_i^{in} that account for the probability of active and inactive individuals with residence in patch i contracting the disease respectively. Importantly, these two terms capture the mixing between contagion processes and recurrent mobility between patches. In the following we describe their functional form.

The term Π_i^{act} in Eqs. (1) and (3) depends on interactions made both inside the household and in the usual workplace of each individual. Taking into account the modified mobility patterns as a result of the outermost layer of intervention, hereinafter denoted by $\widetilde{\mathbf{R}}$, this probability reads as

$$\Pi_i^{act} = 1 - P_{H,i}(t)\sum_{j=1}^{N_P}\widetilde{R}_{ij}(t)P_{O,j}(t), \tag{10}$$

where $P_{H,i}(t)$ and $P_{O,i}(t)$ represent the probability of not contracting the disease at time t inside a household or a workplace located at patch i respectively. The former probability reads as

$$P_{H,i}(t) = \left(1-\beta^I\right)^{z^h\sigma_i\left(\rho_i^P(t)+\rho_i^I(t)\right)}\left(1-\beta^A\right)^{z^h\sigma_i\left(\rho_i^A(t)\right)}. \tag{11}$$

Note that here we assume the number of contacts inside each household to be proportional to its size σ_i and we introduce a scaling factor z_h to ensure that the average number of contacts across the metapopulation matches the estimations obtained from the literature, denoted by $\langle k_h \rangle$. Accordingly

$$z^h = \frac{N\langle k_h \rangle}{\sum_{j=1}^{N_P} n_j\sigma_j}. \tag{12}$$

In its turn, the probability that a susceptible active individual does not contracts the disease inside the patch i at time t, $P_{O,i}(t)$, is given by

$$P_{O,i}(t) = \prod_{j=1}^{N_P}\left(1-\beta^I\right)^{z^Of\left(\frac{n_i^{eff}}{a_i}\right)\frac{n_{j\to i}^P + n_{j\to i}^I}{n_i^{eff}}}\left(1-\beta^A\right)^{z^Of\left(\frac{n_i^{eff}}{a_i}\right)\frac{n_{j\to i}^A}{n_i^{eff}}}, \tag{13}$$

where $n_{j\to i}^P$, $n_{j\to i}^A$ and $n_{j\to i}^I$ are the number of presymptomatic, asymptomatic and infectious agents going from j to i respectively. The effective population of patch i after population movements is encoded as n_i^{eff}. Taking into account the mobility patterns, these quantities can be expressed as

$$n_{j\to i}^m = n_j\rho_j^m(t)p_j(t)\widetilde{R}_{ji}(t), \tag{14}$$

$$n_i^{eff} = \sum_{j=1}^{N_P} n_jp_j(t)\widetilde{R}_{ji}(t). \tag{15}$$

Note that we assume that the contacts of the active population inside each patch i are governed by a monotonically increasing function f_i of

the effective density of each patch i, $d_i^{eff} = n_i^{eff}/a_i$, being a_i its area. In particular, the form chosen for this function is

$$f_i(x) = 2 - e^{-d_i^{eff}/\langle d \rangle}, \tag{16}$$

where $\langle d \rangle$ is the population density across the entire metapopulation. Here the scaling factor z_O is introduced to set the average number of contacts of the active population outside the household to $\langle k_O \rangle$. Therefore

$$z^O = \frac{\langle k_O \rangle \sum_{j=1}^{N_P} n_j^{eff}}{\sum_{j=1}^{N_P} n_j^{eff} f\left(\frac{n_j^{eff}}{a_j}\right)}. \tag{17}$$

Finally, the probability of contracting the disease for the inactive population must only account for the potential contagions occurring when interacting with the household members. Consequently

$$\Pi_i^{in}(t) = 1 - P_{H,i}(t). \tag{18}$$

2.2. Coupling control policies and epidemic dynamics

Mathematically, we couple the socio-economic activity $p_i(t)$ with the fraction of detected residents inside the patch ρ_i^D through a piece-wise function so that

$$p_i(t) = \begin{cases} 1 & if \ \rho_i^D < \varepsilon \\ e^{-\chi\left((\rho_i^D(t)/\varepsilon)-1\right)} & if \ \rho_i^D \geq \varepsilon \end{cases} \tag{19}$$

where χ quantifies the strength of the reaction. Unless specified, we fix $\chi = 10$ ensuring a sharp decrease in the economic activity once the policy is activated. At the metapopulation level, usual mobility patterns, encoded in matrix $\mathbf{R}$, are altered to minimize the interactions with the population from those areas with high incidence numbers ($\rho_j^D > \varepsilon$). From these assumptions, the elements of the modified mobility matrix $\tilde{\mathbf{R}}$ are given by

$$\tilde{R}_{ij}(t) = \begin{cases} p_j(t)R_{ij} & if \ i \neq j \\ 1 - \sum_{j \neq i} p_j(t)R_{ij} & if \ i = j \end{cases} \tag{20}$$

3. Results

To run the Markovian equations in a general scenario, information on the demographic distribution of the population in space, their recurrent mobility patterns, and the structure of their contacts in different contexts is needed to quantify the reduction of sociability as a result of confinement policies. In our particular case, we focus on addressing the spread of diseases across Spanish municipalities with a population of more than 500 individuals. To do so, we extract demographic information from official reports published annually by the National Institute of Statistics of Spain (INE) whereas mobility patterns are obtained by INE from surveys conducted in 2011 in which the population indicated their usual places of work [28]. The information about the average number of contacts a person has per day was obtained from a study reporting the social mixing patterns in 152 countries [29]. As a result, we construct a metapopulation with $N_P = 4293$ patches and $L = 59722$ weighted links. In addition, the epidemiological parameters governing the flows between the different compartments are extracted from the literature and indicated in Table 1.

We first illustrate how the spatiotemporal dynamics of an epidemic outbreak is shaped by the autonomous multiscale control policies here implemented. Unless specified, we use $\varepsilon = 7 \cdot 10^{-4}$, ensuring a rapid

Table 1
Epidemiological parameters and interaction constants. The incubation period is 5.2 days [30] but half of this time infected individuals are not contagious (E stage). The infectious window is the same for both asymptomatic and symptomatic infections ~6.8 days [26]. In the case of the symptomatic individual, this window is divided into P and I stages.

Parameter	Value	Description	Reference
β_I	0.07	$S \xrightarrow{P,I} E$	[26]
β_A	$\beta_I/2$	$S \xrightarrow{A} E$	[26]
η	2.6^{-1}	$E \rightarrow A, P$	[30]
x	0.35	Fraction of symptomatic	[31]
α	2.6^{-1}	$P \rightarrow I$	[26,30]
δ	3^{-1}	$I \rightarrow D$	Assumed
μ_A	6.8^{-1}	$A \rightarrow R$	[26,30]
μ_I	4.2^{-1}	$I \rightarrow R$	[26]
γ	14^{-1}	$D \rightarrow R$	Assumed
$\langle k_H \rangle$	3.2	Average number of contacts at the household	[29]
$\langle k_O \rangle$	8.6	Average number of contacts outside the household	[29]
σ	2.5	Average family members per house	[28]

response of the system when the number of detected symptomatic cases exceeds 70 individuals per 10^5 inhabitants (in the Spanish national health system, the average number of hospital beds per 10^5 people is around 240 [32]). Fig. 2.A represents, for different values of the permeability ϕ, the time evolution of the detected active cases in the 200 most populous municipalities in Spain (grey lines) and the average in the whole country (black line), for an outbreak whose initial seed is placed in the most populous city, Madrid. The emergent self-regulating system leads to different epidemic waves resulting from the activation and deactivation of the control policies to respond to the advance of the outbreak at each municipality. The length and frequency of the epidemic waves are strongly influenced by the social permeability allowed ϕ. High permeability values represent the failure of household isolation, giving rise to a large and long first epidemic wave followed by smaller secondary waves. Instead, when permeability decreases, the creation of social bubbles becomes more successful and we observe a less severe first epidemic wave followed by more frequent and shorter subsequent epidemic outbreaks. In the three scenarios explored, the green lines represent the evolution of the average socioeconomic activity level allowed, $\langle p \rangle(t)$, computed across the different municipalities of the metapopulation. Apart from displaying an anti-phase oscillation with respect to the epidemic waves, comparing the patterns of $\langle p \rangle(t)$ for different values of the permeability ϕ yields a counter-intuitive result: the more stringent local confinements are (the smaller ϕ) the larger socioeconomic activity levels reached.

In the scenarios shown in Fig. 2.A the number of active detected cases falls above the desirable incidence of the disease as a result of the existence of different infectious compartments inducing a lag between the deployment of an intervention and its observed outcome. The creation of social bubbles entails an instantaneous depletion of the pool of susceptible individuals, making those living in healthy households unreachable for other infectious peers. This is translated into an abrupt decrease in the effective reproduction number $\mathcal{R}$, allowing the *suppression* of the outbreak. In the absence of social bubbles, all the individuals are exposed to the disease, but the outbreak advances with lower speed due to the reduced sociability, corresponding to a *mitigation* strategy.

In epidemiological terms, Fig. 2.B shows that the distribution of the value of the first epidemic peaks of all Spanish municipalities is reduced as the permeability ϕ decreases, i.e. as the stringency of the local control policy increases. Obviously, larger values of the first peak result in a higher contribution to the overall attack rate, which explains the small amplitude of the subsequent epidemic waves for large values of ϕ as a result of the reduced susceptible population that remains.

The economic outcome of the different control policies is shown in Fig. 2.C. Each bar in the histogram represents the share of time during which the population of each municipality maintains a given level of
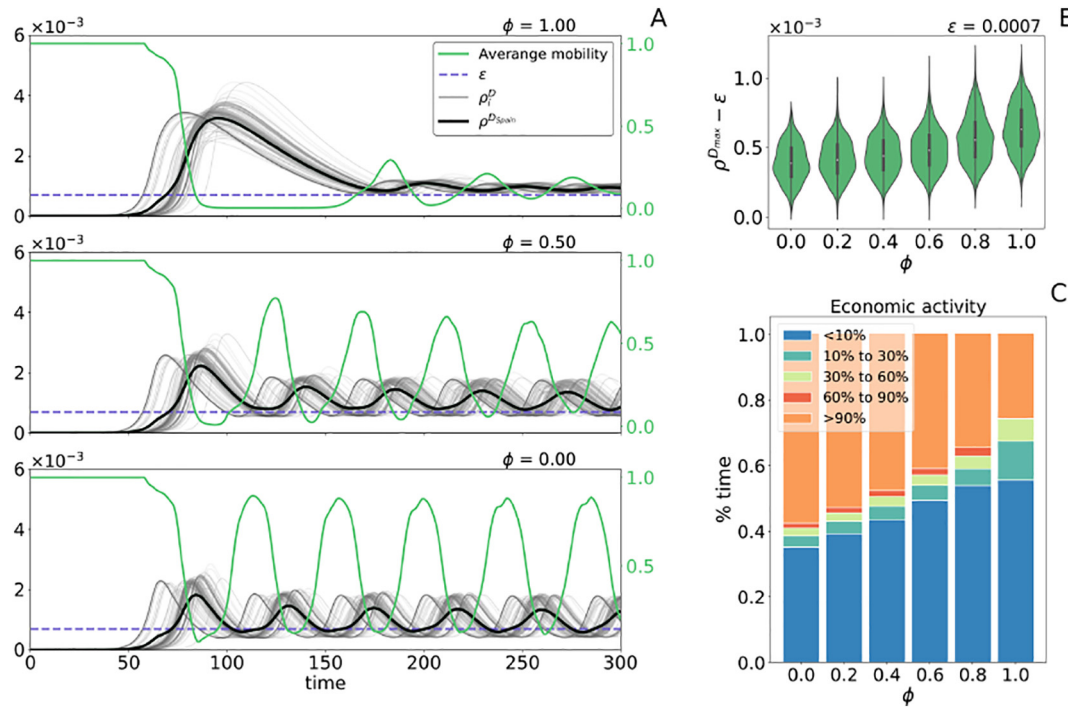
Fig. 2. Epidemic evolution & socioeconomic activities. A. Evolution of symptomatic detected individuals (black and grey lines) and the mean value of the socioeconomic activity level $\langle p \rangle$ (green line) for three different permeability values. Grey lines represent the evolution for the 200 most populous Spanish cities, whereas the black line shows the average number of detected individuals at the national level. The dashed line represents the value of the tolerance threshold ε. B. Distribution of the maximum value of detected individuals in each municipality for different values of ϕ. C. Distribution of the activity level allowed over 300 days for different permeability values.

economic activity corresponding to different ranges of p values. This plot highlights the effect that was observed in the evolution of $\langle p \rangle(t)$ in the different panels of Fig. 1.A (green lines): short and strict control policies are more beneficial in economic terms than long and lax interventions. This result shows that it is possible to strike a trade-off between controlling an outbreak while minimizing the economic cost of the intervention by implementing stringent measures at the local level.

Once shown the role of the stringency of local control policies plays in the success of multiscale NPIs implemented, we now explore the interplay between a particular mobility network of the population and the aforementioned local measures. In other words, we aim at answering the following question: How does the interconnectivity between the different urban areas affect the outcome of the reactive policies for different permeability values? To do so, we run our model independently for the different highest administrative divisions of Spain, the autonomous communities. Note that, by dividing the national territory, we do not lose a relevant part of the information, since only the 2% of the total volume of daily flows involves movementes between different autonomous communities. From a political point of view, this administrative separation is also relevant for the design and planning of containment policies in Spain, given that health competencies, and therefore the deployment of control policies and the distribution of health resources, are in the hands of these territories.

To get some insights into the role of the mobility network, we first reproduce the analysis shown in Fig. 2A but now focusing on each individual autonomous community. Specifically, we set $\phi=0$, i.e. perfect household isolation, place an infectious seed in the most populous city and represent in Fig. 3A the spatio-temporal distribution of detected cases in each territory along with the average socio-economic activity level. Interestingly, we observe important heterogeneities concerning the shape of the different epidemic waves in each territory: while autonomous communities like Cantabria and the Community of Madrid are characterized by very synchronized epidemic curves triggering a sharp coherent collective evolution, the outbreaks in municipalities

located in other areas such as Canary Island display important time lags leading to less coherent epidemic waves. These heterogeneities become more evident in Fig. 3B, where we represent the time distribution of the position of the first epidemic peak inside each autonomous community, finding important differences in terms of their variance.

From a systemic perspective, the synchronization of the individual epidemic curves has deep implications for the temporal evolution of the overall number of cases in the entire metapopulation. To check this hypothesis, we represent in Fig. 4A how the magnitude of the peak of individuals detected in the first epidemic wave evolves as a function of the social permeability allowed for each autonomous community. Interestingly, we observe how this indicator, somehow related to the highest expected burden to the health system over the course of the disease, strongly varies between the different territories of Spain. Specifically, the affordable permeability values to keep the cumulative incidence over 14 days below 240 cases per 10^5 inhabitants range from $\phi^{aff}=0.06$ for the Community of Madrid to $\phi^{aff}=0.67$, corresponding to the Balearic Islands.

The heterogeneity between different territories observed in the former analysis reveals that the different scales governing the reaction-diffusion processes that cause the spatial diffusion of an epidemic outbreak are highly intertwined. As a result, the outcome of the local policies, such as the modulation of the economic activity regulated by $p(t)$ or the social bubbles mechanism governed by ϕ, are highly influenced by global aspects such as the demographic distribution of the population or how they move across a given territory. Qualitatively, we observe a coherent epidemic wave inside those territories requiring more strict policies (smaller ϕ^{aff} values). In contrast, the municipalities located in those autonomous communities for which loose policies are affordable exhibit an asynchronous evolution. As a consequence, the internal policies are activated at different times across the territory, allowing a progressive control of the outbreak, which results in the flattening of the aggregated epidemic curve and explains the lower magnitude of the peak.
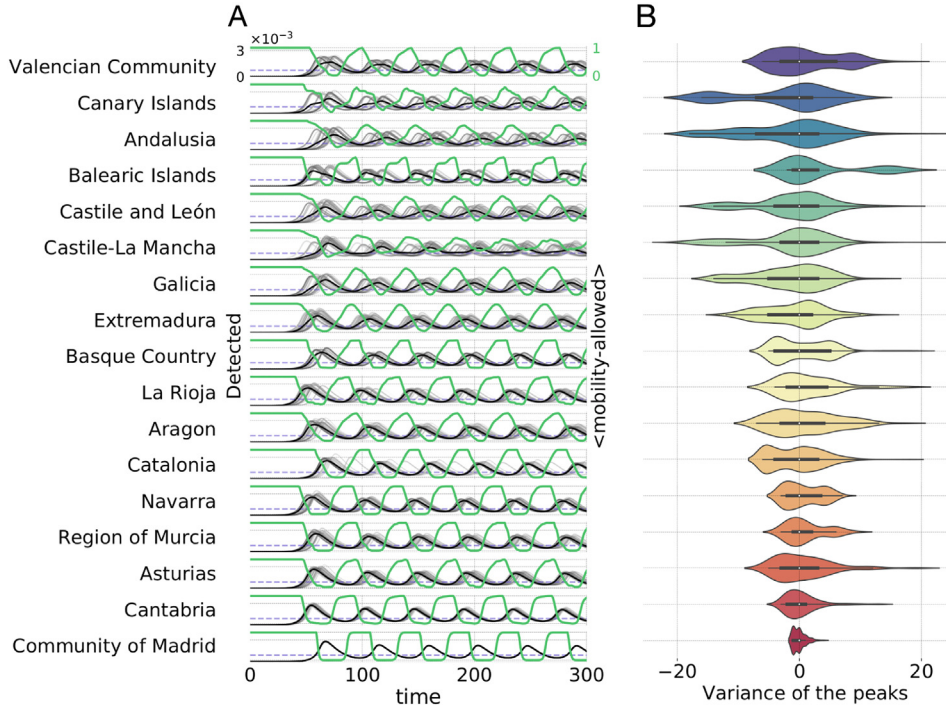
Fig. 3. Epidemic wave synchronization for different metapopulation structures. A. The violin plots represent the time variance of the subpopulations (municipalities) reaching the peak of the epidemic wave for each autonomous communities of Spain. The colors represent from red to purple from the worst to the best relative epidemic outcome respectively for all Spanish autonomous communities for null permeability value. B. Epidemic time evolution of the infected and detected for $\phi=0$, the grey lines are the 50 most populous municipalities of each autonomous community and in black the average. The green lines represent the average mobility in the autonomous community.

Finally, we aim at finding a heuristic argument to connect the features of the underlying metapopulation with the affordable permeability values for each territory. Providing an initial infectious individual is seeded in a single patch, the degree of coherence observed for the time evolution of the ensemble of municipalities in each territory has to be related to the communication of the source of infection with the rest of the network through the population movements. To find such a relation, we first define a new matrix **M** whose elements M_{ij} determines the expected number of interactions of one individual placed in patch i with the population living in patch j. Specifically, under the model assumptions, these elements read [33]

$$M_{ij} = \sum_{l=1}^{N_P} R_{il} f_l \frac{n_j R_{jl}}{\tilde{n}_l}. \tag{21}$$

In dynamical terms, it seems logical to assume that a strong interaction between two patches, as dictated by the matrix **M**, boosts the diffusion of infectious individuals across them. Therefore, we can define a proximity measure d_{ij} between two patches i and j as

$$d_{ij} = M_{ij}^{-1}. \tag{22}$$

Note that the elements d_{ij} somehow reflect the time taken by an epidemic outbreak, seeded in patch i, to invade patch j. Our
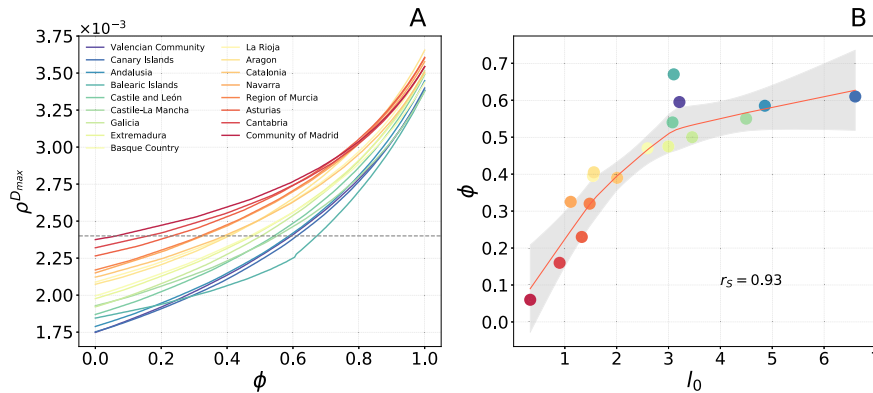

Fig. 4. Permeability, saturation of the health system & structural correlations. A. *Maximum* number of detected individuals during the first epidemic wave ρ^{Dmax} as a function of the social permeability ϕ allowed for each autonomous region. The dashed line indicates the threshold used, 2.4×10^{-3}, to calculate the permeability that can be afforded by each territory. B. Correlation between the affordable permeability of each community ϕ^{aff} and the average shortest contagion path connecting a random individual with the infection source in each territory l_0. Solid red line shows the LOESS regression of the data whereas the shadowed region showed the 95% confidence interval obtained by bootstrapping 1000 samples.

hypothesis is that the degree of synchronization of the epidemic curves from the different autonomous communities, and consequently their affordable permeability, can be inferred from the structural features of the matrix $\mathbf{d}$. Namely, shorter effective distances from every single node of the metapopulation to the source of the outbreak should give rise to a higher degree of synchronization. Following this rationale, we define our structural metric l_0 as the average shortest path length connecting a randomly picked individual with the source of an outbreak over the proximity matrix $\mathbf{d}$. Accordingly:

$$l_0 = \frac{\sum_{i=1}^{N_P} n_i l_{i0}}{\sum_{i=1}^{N_P} n_i},$$

(23)

where l_{i0} constitutes the shortest path length connecting the location i with the source of the outbreak in the proximity matrix $\mathbf{d}$. We represent in Fig. 4B the affordable permeability ϕ^{aff} as a function of the value of this metric for each autonomous community, finding a strong positive correlation between both indicators. Moreover, the LOESS regression of the data yields a monotonically increasing function relating ϕ^{aff} and l_0. Taken together, these results indicate that regions with dispersed mobility networks may not require local control policies as strict as densely communicated territories.

4. Conclusions

The rapid spread of COVID-19 during the early months of 2020 caused the world to face a recession on a scale not seen since the Great Depression [7,8]. Despite the vaccination breakthrough achieved during 2021, its uneven global coverage and the emergence of new variants have prolonged the health and economic crisis to date, successively producing epidemic waves that have continued to overwhelm healthcare systems with the resulting loss of millions of lives. Throughout this time, governments have tried to control the spread of SARS-CoV-2 with various contention measures such as mass testing and contact tracing, reinforcement of prophylactic measures such as social distancing and face mask use [2], and of course vaccination [9]. Despite the success of the former policies, many countries have been forced to implement again massive confinements of the population when the epidemiological situation has escaped their control [4]. Therefore, maintaining the difficult trade-off between the social functioning of a country and the relief of the overwhelmed health systems requires a structured policy that adapts to the population's needs at any given moment.

In this paper, we have analyzed the control capacity of reactive policies that implement containment measures when the epidemiological situation exceeds a certain tolerance threshold. The different measures implemented act at multiple scales: at the global level, mobility decreases to and from high-incidence areas, at each patch the economic activity decreases and, at the household level, social bubbles are created, shielding the susceptible living with non-infectious individuals.

The effectiveness of the former measures depends on the degree of severity of the measures adopted and the social adhesion to them. This way, our analyses have focused on how the severity of measures at the local level influences the ability to control epidemic waves. In this regard, our work yields three main results. First, as expected, a higher stringency of local measures facilitates the control provided by the policies implemented at larger scales, resulting in a train of epidemic waves manageable from a health point of view rather than a huge first epidemic outbreak. Secondly, we note how, in addition to serving better outbreak management, the implementation of stringent measures counter-intuitively provides less disruption to the socio-economic fabric as societies can afford more periods of normal activity than in the case of lax implementation of local measures.

Finally, the most interesting result has been obtained when analyzing how the social architecture, here represented by the demographic spatial distribution and the human mobility network, influences the severity of local rules needed to achieve a given control of the epidemic. By focusing on the different autonomous communities of Spain, we have shown that their different architectures are determining (decisive) for the outcome of the spreading behavior and its control. In particular, while some autonomous communities should be more aggressive with local restrictions, forcing household isolation to more than 95% of the population, others may allow a certain degree of local activity as they only need that around 35% of individuals are inside safe social bubbles. To explain the heterogeneity in the stringency of local restrictions needed, we have relied on a new metric that combines the different aspects of social mixing that interplay in a metapopulation. In particular, by computing the average contagion distance between the infected seed and any potential susceptible individual, we have shown that those autonomous communities for which this distance is small are the ones that need more stringent measures at the local level to achieve the desired epidemic control. Naturally, this result is manifested in the synchronous epidemic dynamics observed for territories with a small contagion distance: the more synchronized epidemic waves of individual patches are, the more restrictive local measures should be.

To round off, our analysis of independent multiscale reactive policies has highlighted that the social structure underlying the mixing of individuals greatly influences the stringency of local measures needed to tackle the control of epidemic waves. Our analysis has focused on the case of Spain where, since August 2020, the government left the implementation of control measures in the hands of the autonomous communities. This delegation of functions to the autonomous communities has given rise to different ways of managing the four epidemic waves that have emerged since that date, these being strongly influenced by the particular ideology of the party governing each community. Although our framework constitutes a first approximation to more refined models of epidemic containment, the heterogeneity found for the stringency required for containment in the different autonomous communities shows that control policies should be carefully devised taking into account the social architecture of each territory.

Declaration of competing interest

The authors declare that they have no known competing financial interests or personal relationships that could have appeared to influence the work reported in this paper.

Acknowledgments

References

[1] Bo Y, Guo C, Lin C, Zeng Y, Li HB, Zhang Y, Hossain MS, Chan JW, Yeung DW, Kwok KO, et al. Effectiveness of non-pharmaceutical interventions on covid-19 transmission in 190 countries from 23 january to 13 april 2020. Int J Infect Dis. 2021;102: 247–53.

[2] Hale T, Angrist N, Goldszmidt R, Kira B, Petherick A, Phillips T, Webster S, Cameron-Blake E, Hallas L, Majumdar S, Tatlow H. A global panel database of pandemic

policies (oxford covid-19 government response tracker). Nat Hum Behav. 2021;5: 529–38.

[3] Perra N. Non-pharmaceutical interventions during the covid-19 pandemic: a review. Phys Rep. 2021;913:1–52.

[4] COVID-19 stringency index. https://ourworldindata.org/grapher/covid-stringency-index.

[5] Laing T. The economic impact of the coronavirus 2019 (covid-2019): implications for the mining industry. Ext Ind Soc. 2020;7(2):580–2.

[6] Ong R. Covid-19: Remittance flows to shrink 14% by 2021. The world bank; 2020.

[7] Verma P, Dumka A, Bhardwaj A, Ashok A, Kestwal MC, Kumar P. A statistical analysis of impact of covid19 on the global economy and stock index returns. SN Comput Sci. 2021;2(1):27.

[8] Gopinath G. The great lockdown: worst economic downturn since the great depression. IMF Blog. 2020;14:2020.

[9] Mathieu E, Ritchie H, Ortiz-Ospina E, Roser M, Hasell J, Appel C, Giattino C, Rodés-Guirao L. A global database of covid-19 vaccinations. Nat Hum Behav. 2021;5(7): 947–53. https://doi.org/10.1038/s41562-021-01122-8. URL.

[10] N. Cumming-Bruce, Unequal vaccine access is widening the global economic gap, a u.n. agency says., https://www.nytimes.com/2021/10/27/world/united-nations-coronavirus.html.

[11] Bernal JLopez, Andrews N, Gower C, Gallagher E, Simmons R, Thelwall S, Stowe J, Tessier E, Groves N, Dabrera G. Effectiveness of covid-19 vaccines against the b. 1.617. 2 (delta) variant. N Engl J Med. 2021:585–94.

[12] Pfizer, BioNTech. Pfizer and biontech provide update on omicron variant. https://www.pfizer.com/news/press-release/press-release-detail/pfizer-and-biontech-provide-update-omicron-variant.

[13] N. Haug L. Geyrhofer A. Londei E. Dervic A. Desvars-Larrive V. Loreto B. Pinior S. Thurner P. Klimek, Ranking the effectiveness of worldwide covid-19 government interventions, Nat Hum Behav

[14] Acemoglu D, Chernozhukov V, Werning I, Whinston MD. A multi-risk SIR model with optimally targeted lockdown. , Vol. 2020MA: National Bureau of Economic Research; 2020..

[15] Acemoglu D, Chernozhukov V, Werning I, Whinston MD. Optimal targeted lockdowns in a multigroup sir model. Am Econ Rev Insights. 2021;3(4):487–502.

[16] Brotherhood L, Kircher P, Santos C, Tertilt M. An economic model of the covid-19 epidemic: the importance of testing and age-specific policies; 2020..

[17] Meidan D, Schulmann N, Cohen R, Haber S, Yaniv E, Sarid R, Barzel B. Alternating quarantine for sustainable epidemic mitigation. Nat Commun. 2021;12(1):220. https://doi.org/10.1038/s41467-020-20324-8. URL.

[18] Della Rossa F, Salzano D, Di Meglio A, De Lellis F, Coraggio M, Calabrese C, Guarino A, Cardona-Rivera R, De Lellis P, Liuzza D, Lo Iudice F, Russo G, di Bernardo M. A network model of italy shows that intermittent regional strategies can alleviate the covid-19 epidemic. Nat Commun. 2020;11(1):5106. https://doi.org/10.1038/s41467-020-18827-5.

[19] Silva PC, Batista PV, Lima HS, Alves MA, Guimarães FG, Silva RC. Covid-abs: an agent-based model of covid-19 epidemic to simulate health and economic effects of social distancing interventions. Chaos Solitons Fractals. 2020;139:110088https://www.sciencedirect.com/science/article/pii/S0960077920304859.

[20] Faucher B, Assab R, Roux J, Levy-Bruhl D, Kiem CT, Cauchemez S, Zanetti L, Colizza V, Boëlle P-Y, Poletto C. Reactive vaccination of workplaces and schools against covid-19. medRxiv; 2021..

[21] Yan Y, Malik AA, Bayham J, Fenichel EP, Couzens C, Omer SB. Measuring voluntary and policy-induced social distancing behavior during the covid-19 pandemic. Proc Natl Acad Sci. 2021.;118(16) arXiv:https://www.pnas.org/content/118/16/e2008814118.full.pdf. https://www.pnas.org/content/118/16/e2008814118.

[22] De Meijere G, Colizza V, Valdano E, Castellano C. Effect of delayed awareness and fatigue on the efficacy of self-isolation in epidemic control. Phys Rev E. 2021; 104:044316.

[23] Gómez-Gardeñes J, Soriano-Panos D, Arenas A. Critical regimes driven by recurrent mobility patterns of reaction–diffusion processes in networks. Nat Phys. 2018;14 (4):391–5.

[24] Granell C, Mucha PJ. Epidemic spreading in localized environments with recurrent mobility patterns. Phys Rev E. 2018;97(5):052302.

[25] Estrada E. Covid-19 and sars-cov-2. Modeling the present, looking at the future. Phys Rep. 2020;869:1–51.

[26] Arenas A, Cota W, Gómez-Gardeñes J, Gómez S, Granell C, Matamalas JT, Soriano-Paños D, Steinegger B. Modeling the spatiotemporal epidemic spreading of COVID-19 and the impact of mobility and social distancing interventions. Phys Rev X. 2020;10:041055https://link.aps.org/doi/10.1103/PhysRevX.10.041055.

[27] Gómez S, Arenas A, Borge-Holthoefer J, Meloni S, Moreno Y. Discrete-time markov chain approach to contact-based disease spreading in complex networks. Europhys Lett. 2010;89(3):38009.

[28] Instituto Nacional de Estadística. Demographics and mobility patterns. https://www.ine.es; 2021.

[29] Prem K, Cook AR, Jit M. Projecting social contact matrices in 152 countries using contact surveys and demographic data. PLoS Comput Biol. 2017;13(9):e1005697.

[30] Lauer SA, Grantz KH, Bi Q, Jones FK, Zheng Q, Meredith HR, Azman AS, Reich NG, Lessler J. The incubation period of coronavirus disease 2019 (covid-19) from publicly reported confirmed cases: estimation and application. Ann Intern Med. 2020; 172(9):577–82.

[31] COVID-19 pandemic planning scenarios, //www.cdc.gov/coronavirus/2019-ncov/hcp/planning-scenarios.html.

[32] National Helath System capacity of Spain, https://www.mscbs.gob.es/estadEstudios/sanidadDatos/tablas/tabla22.htm.

[33] Hazarie S, Soriano-Paños D, Arenas A, Gómez-Gardeñes J, Ghoshal G. Interplay between population density and mobility in determining the spread of epidemics in cities. Commun Phys. 2021;4(1):1–10.